

Infrared Spectra and Ab Initio Calculations for the $F^-(CH_4)_n$ ($n = 1-8$) Anion Clusters

Z. M. Loh, R. L. Wilson, D. A. Wild, and E. J. Bieske*

School of Chemistry, The University of Melbourne, Australia 3010

J. M. Lisy

Department of Chemistry, University of Illinois at Urbana-Champaign, Urbana, Illinois 61801

B. Njagic and M. S. Gordon*

Department of Chemistry, Iowa State University, Ames, Iowa 50011

Received: August 22, 2006; In Final Form: October 18, 2006

Infrared spectra of mass-selected $F^-(CH_4)_n$ ($n = 1-8$) clusters are recorded in the CH stretching region (2500–3100 cm^{-1}). Spectra for the $n = 1-3$ clusters are interpreted with the aid of ab initio calculations at the MP2/6-311++G(2df 2p) level, which suggest that the CH_4 ligands bind to F^- by equivalent, linear hydrogen bonds. Anharmonic frequencies for CH_4 and F^-CH_4 are determined using the vibrational self-consistent field method with second-order perturbation theory correction. The $n = 1$ complex is predicted to have a C_{3v} structure with a single CH group hydrogen bonded to F^- . Its spectrum exhibits a parallel band associated with a stretching vibration of the hydrogen-bonded CH group that is red-shifted by 380 cm^{-1} from the ν_1 band of free CH_4 and a perpendicular band associated with the asymmetric stretching motion of the nonbonded CH groups, slightly red-shifted from the ν_3 band of free CH_4 . As n increases, additional vibrational bands appear as a result of Fermi resonances between the hydrogen-bonded CH stretching vibrational mode and the $2\nu_4$ overtone and $\nu_2 + \nu_4$ combination levels of the methane solvent molecules. For clusters with $n \leq 8$, it appears that the CH_4 molecules are accommodated in the first solvation shell, each being attached to the F^- anion by equivalent hydrogen bonds.

1. Introduction

Ion–molecule complexes and clusters are computationally and experimentally tractable systems for exploring solvation on a microscopic level. In this regard, anion clusters composed of a halide anion “solvated” by one or more second-row hydride molecules have served as important prototype systems to elucidate the importance of solute–solvent and solvent–solvent bonds in deciding cluster structures. On the experimental front, earlier thermochemical studies^{1,2} in which binding enthalpies for the solvent molecules were measured have recently been complemented by infrared spectroscopic studies of size-selected clusters. Ever more sophisticated ab initio investigations have paralleled the experimental work, delivering predictions for geometrical structures, vibrational frequencies and intensities, and ligand binding energies.^{1,3–10} The infrared spectroscopic targets have included clusters comprising a halide anion (F^- , Cl^- , Br^- , I^-) solvated by one or more molecules (CH_4 ,^{11–14} NH_3 ,¹⁵ H_2O ,^{16–22} HF ,^{23–25} C_2H_2 ,^{26–28} CH_3OH ,^{29,30} C_2H_5OH ,³¹ and C_3H_7OH ,³¹ $HCOOH$,³² C_2H_4 ,³³ and CO_2 ³⁴).

In this article, we report IR spectra of size-selected $F^-(CH_4)_n$ ($n = 1-8$) clusters to help understand the way in which a fluoride anion is progressively solvated by methane molecules. To support the spectroscopic studies, minimum-energy structures and vibrational frequencies for the $n = 1-3$ clusters are determined through ab initio calculations. Comparisons between calculated and measured CH stretching vibrational frequencies and intensities are used to establish links between IR spectra and cluster structures.

Previous spectroscopic and theoretical studies demonstrate that the F^-CH_4 , Cl^-CH_4 , and Br^-CH_4 dimers have C_{3v} structures with the halide anion attached to a CH group of the CH_4 molecule.^{2,4,11–13} Infrared and computational investigations of larger $Cl^-(CH_4)_n$ ($n = 1-10$) clusters suggest that methane acts as a relatively simple solvent molecule for halide anions.¹⁴ Each CH_4 molecule is H bonded to the Cl^- core, whereas weaker $CH_4 \cdots CH_4$ dispersion interactions encourage the methane molecules to clump together. It is likely that $F^-(CH_4)_n$ clusters adopt similar solvation structures, although because of the smaller ionic radius of F^- , it is possible that fewer CH_4 molecules are accommodated in the first solvation shell about F^- than about Cl^- .

Some insight into the solvation structures and energetics of the $F^-(CH_4)_n$ clusters is provided by earlier thermochemical measurements for the clustering equilibria,²



Association enthalpies for the $n = 1-10$ clusters (plotted in Figure 1) decrease regularly with n , with small, abrupt drops occurring between $n = 6$ and 7 and between $n = 8$ and 9. These drops were tentatively taken to indicate that $n = 6$ corresponds to the filling of an octahedral inner solvent shell and that the seventh and eighth CH_4 ligands fit into two opposite C_{3v} pockets of the $F^-(CH_4)_6$ octahedral structure. In principle, IR spectra of the $F^-(CH_4)_n$ clusters should provide complementary structural information because of the sensitivity of the CH_4

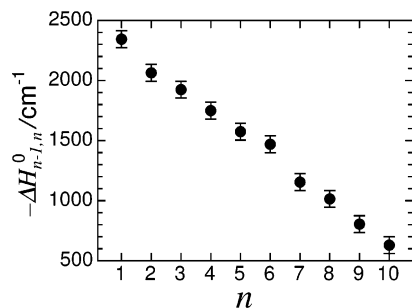


Figure 1. Association enthalpies for F⁻-(CH₄)_n clustering reactions (from ref 2). Quoted uncertainties are ±70 cm⁻¹.

ligand's vibrational frequencies and intensities to their hydrogen-bonding environments.

2. Experimental and Theoretical Methods

Infrared spectra of F⁻-(CH₄)_n clusters were obtained by scanning the IR wavelength over the CH stretching region while monitoring the production of ion photofragments. Following the excitation of a CH stretching mode, energy migrates into a weak intermolecular bond, leading to its rupture and to the liberation of F⁻-(CH₄)_{n-m} photofragments. The *n* - 1 fragment channel was monitored for *n* ≤ 4, and the *n* - 2 channel was monitored for *n* > 4. The photodissociation strategy should be suitable for observing the CH stretching transitions (2500–3100 cm⁻¹ range) of cold F⁻-(CH₄)_n clusters because the energy required to remove a single CH₄ molecule is less than 2400 cm⁻¹.²

The apparatus consists of a tandem mass spectrometer equipped with a source for generating cooled cluster ions. The F⁻-(CH₄)_n clusters were produced in an electron beam-crossed supersonic expansion of a 1% CH₄/Ar mixture (for F⁻-CH₄) or neat CH₄ (for larger clusters) seeded with NF₃ as the F⁻ ion precursor. Optimal cluster formation required having a relatively small separation between the nozzle orifice and electron impact zone, suggesting that CH₄ molecules attach to the F⁻ ions through three-body association reactions in the early zone of the expansion.

The tandem mass spectrometer comprises a primary quadrupole filter for selection of the parent F⁻-(CH₄)_n ions, an octopole ion guide, where the ions were overlapped with the counter-propagating output of a pulsed, tunable IR radiation source (Nd:YAG pumped optical parametric oscillator Continuum Mirage 3000, 0.017 cm⁻¹ bandwidth), and a second quadrupole filter tuned to the mass of the charged photofragment. Photofragments were sensed with a microsphere plate. Wavelength calibration was accomplished using a wavemeter (New Focus 7711) to measure the wavelength of the signal output from the OPO's first stage and the seeded Nd:YAG laser's 532 nm output. Reference 27 gives further details of the experimental setup.

Ab initio calculations for F⁻-(CH₄)_n, *n* = 1–3, were performed at the MP2/6-311++G(2df 2p) level using GAMESS software³⁵ to provide structures and vibrational frequencies. Only the valence electrons were correlated. Anharmonic frequencies for CH₄ and F⁻-CH₄ were determined using the vibrational self-consistent field method with second-order perturbation theory correction.³⁶

3. Theoretical Results

3.1. Calculated Cluster Structures for F⁻-(CH₄)_n (*n* = 1–3). Figure 2 shows calculated equilibrium structures of the *n* = 1–3 complexes. As in previous theoretical studies,^{4,13} the

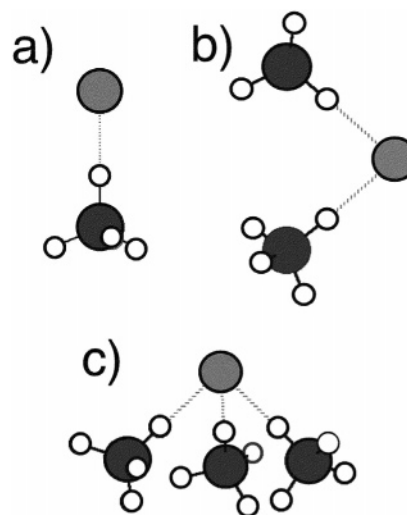


Figure 2. Minimum-energy structures for the F⁻-(CH₄)_n (*n* = 1–3) complexes calculated at the MP2/6-311++G(2df 2p) level.

F⁻-CH₄ dimer is predicted to adopt a C_{3v} structure with a single, linear hydrogen bond (F⁻-H_b separation of 1.840 Å). The CH₄ subunit is slightly distorted through its interaction with F⁻, most notably by a small increase in the length of the H-bonded CH group (0.025 Å). A similar F⁻⋯CH₄ H-bonding motif is preserved in the *n* = 2 and 3 clusters. For F⁻-(CH₄)₂, the optimized structure has C₂ symmetry with two equivalent methane ligands adjacent to one another and a H_b-F-H_b bond angle of φ = 87° (Figure 2b). The F⁻-(CH₄)₃ cluster is predicted to have a pyramidal C₃ structure with three equivalent CH₄ ligands attached to the F⁻ ion (H_b-F-H_b bond angle φ = 83°) (Figure 2c). The non-H-bonded CH groups in both F⁻-(CH₄)₂ and F⁻-(CH₄)₃ are predicted to be interleaved in a cog-type fashion. Structures in which the methane ligands are H bonded to one side of the halide are presumably favored because of attractive CH₄⋯CH₄ dispersion interactions and because the H-bonded CH groups can concertedly polarize the halide anion, stabilizing the intermolecular bonds.

Computed energies for loss of a single CH₄ molecule from F⁻-(CH₄)_n, *n* = 1–3, (6.92, 5.70, and 4.89 kcal/mol, including harmonic zero-point energy corrections) agree well with measured association enthalpies (6.7, 5.9, and 5.5 kcal/mol).² The trend is consistent with the expectation that the F⁻⋯CH₄ H bonds weaken as more CH₄ molecules are attached to the F⁻. There is a corresponding increase in the F⁻⋯H_b separation (1.840, 1.930, and 1.957 Å for *n* = 1–3), a slight decrease in the length of the H-bonded CH group (1.109, 1.103, and 1.099 Å for *n* = 1–3) and, as discussed below, an increase in the frequency of the H-bonded CH stretching mode.

Although the *n* = 1–3 structures shown in Figure 2 were the only locatable minima at the MP2/6-311++G(2df 2p) level, it should be noted that the clusters are extremely floppy, particularly in the coordinates corresponding to torsional motion of the CH₄ subunits about the F⁻⋯CH₄ intermolecular bonds. Ab initio energy calculations for F⁻-(CH₄)₂, in which one of the methyl groups was fixed and the other was rotated, suggest that the methyl rotation barrier is tiny (<10 cm⁻¹) and of the same order of magnitude as the methane rotational constant (5.2 cm⁻¹). For the finite energy clusters probed experimentally, the methane subunits probably behave as almost free rotors.

To gauge how easily the CH₄ ligands can move around the F⁻, a bending potential energy curve was calculated at the MP2/6-311++G(2df 2p) level for F⁻-(CH₄)₂. The H_b-F-H_b angle (φ) was stepped in increments of 15° while allowing remaining

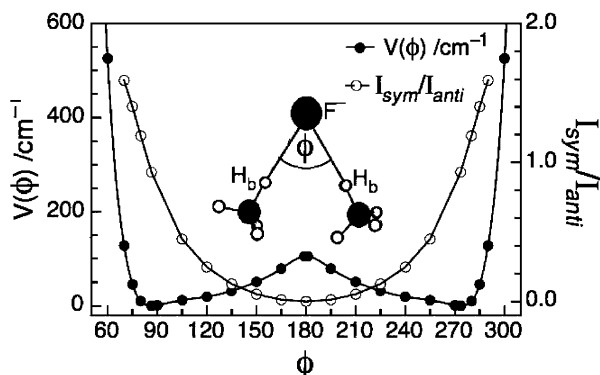


Figure 3. Potential energy curve (solid points) for the lowest-energy intermolecular bending motion of $F^-(CH_4)_2$. The minimum corresponds to $\phi = 87^\circ$. Also plotted is the ratio of the intensities for the symmetric and antisymmetric $\nu_{hb}(a_1)$ stretches as a function of ϕ (hollow points).

co-ordinates to relax. The resulting potential energy curve, shown in Figure 3, has its minimum at $\phi = 87^\circ$ and rises sharply when the two CH_4 molecules are brought together, presumably because of overlap repulsion. The system can move from the $\phi = 87^\circ$ minimum to a linear configuration ($\phi = 180^\circ$) at an energy cost of $\sim 100\text{ cm}^{-1}$, only slightly less than the intermolecular bond energy for the $(CH_4)_2$ dimer ($\sim 130\text{ cm}^{-1}$).^{37–40} It is quite possible that the intermolecular methane–methane bonds are effectively broken in the clusters probed experimentally.

3.2. Calculated Harmonic Vibrational Frequencies. Harmonic vibrational frequencies were calculated at the MP2/6-311++G(2df 2p) level for the $n = 1–3$ clusters. The results are available as Supporting Information to this article. We first consider the CH stretching modes of the clusters. The bare CH_4 molecule has two CH stretching modes: the IR-active triply degenerate $\omega_3(t_2)$ mode and the IR-inactive totally symmetric $\omega_1(a_1)$ mode. In the F^-CH_4 dimer, the $\omega_3(t_2)$ mode is resolved into two modes, one of which, denoted $\omega_3(a_1)$, is IR weak and corresponds to the symmetric stretching motion of the three nonbonded CH groups. The other vibration, an asymmetric stretching motion of the nonbonded CH groups, denoted $\omega_3(e)$, is doubly degenerate and strongly IR-active. The $\omega_1(a_1)$ symmetric stretching mode of CH_4 (IR-inactive) is transformed into a strongly IR-active mode, denoted $\omega_{hb}(a_1)$, which principally entails stretching of the H-bonded CH group. This vibration is significantly red-shifted from the $\omega_1(a_1)$ mode of the free CH_4 molecule with the magnitude of the red-shift correlated with the H-bond strength. The $\omega_3(e)$ and $\omega_3(a_1)$ modes are also slightly red-shifted from the CH stretches of free CH_4 because they also involve some stretching displacement of the H-bonded CH group.

The CH stretching and bending modes of $F^-(CH_4)_2$ and $F^-(CH_4)_3$ occur in groups analogous to those of F^-CH_4 , a consequence of the fact that the F^- anion is the major perturbing influence on the attached CH_4 subunits. The evolution of the CH stretching vibrational frequencies is shown for the $F^-(CH_4)_n$ ($n = 1–3$) clusters in Figure 4. Generally, the CH stretching vibrations shift to a higher frequency as n increases, reflecting the weakening of the intermolecular H bonds.

The CH stretching modes of $F^-(CH_4)_2$ can be described in terms of symmetric and antisymmetric combinations of equivalent vibrational motions localized on the CH_4 subunits. For example, there are symmetric and antisymmetric combinations of the H-bonded CH stretches localized on each of the CH_4 subunits. Both combinations have appreciable IR intensities

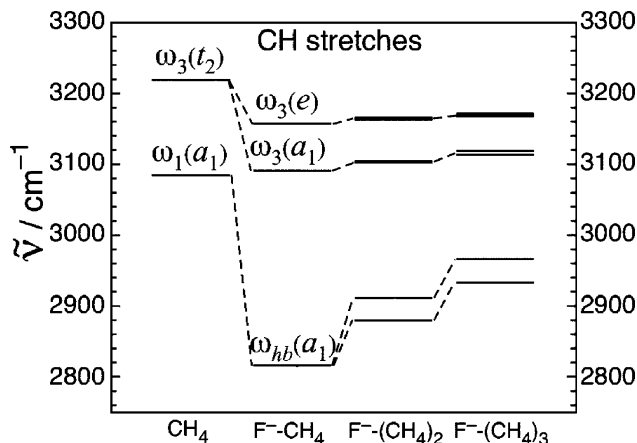


Figure 4. Calculated harmonic CH stretching vibrational frequencies for CH_4 , F^-CH_4 , $F^-(CH_4)_2$, and $F^-(CH_4)_3$. Note the transformation of the $\omega_3(t_2)$ mode of CH_4 to the $\omega_3(a_1)$ and $\omega_3(e)$ modes of F^-CH_4 as the symmetry is reduced from T_d to C_{3v} , and also the significant frequency reduction of $\omega_1(a_1)$ as it is transformed into the H-bonded CH stretching mode $\omega_{hb}(a_1)$.

(9.20 and $9.92\text{ D}^2/\text{amu}\cdot\text{\AA}^2$) and possess slightly different frequencies (2911 and 2879 cm^{-1}) because of coupling through the light F^- anion. Similar symmetric and antisymmetric combinations occur for the other methane-localized stretching and bending vibrations but in each case differ in frequency by $< 5\text{ cm}^{-1}$. Equivalent groupings pertain to $F^-(CH_4)_3$. For example, the three local H-bonded CH stretching vibrations combine to give one concerted, in-phase stretching mode (a_1 symmetry, 2965 cm^{-1}) and one doubly degenerate mode (e symmetry, 2933 cm^{-1}). In the remainder of this article, we continue to label the CH_4 -localized vibrations for larger clusters ($n > 1$) according to the designations for F^-CH_4 , making explicit mention of the n different combinations only when necessary to avoid ambiguity.

The low-frequency intermolecular motions ($< 300\text{ cm}^{-1}$) for $n = 1–3$ clusters involve, in order of decreasing frequency, intermolecular bends and stretches (for $n = 1–3$), bending motions in which the CH_4 subunits move about the F^- (for $n = 2, 3$), and torsional modes (for $n = 2, 3$). As noted above (section 3.1), the torsional and low-frequency bending modes are expected to be extremely anharmonic, involving large excursions, and will be poorly described by the harmonic frequency calculations.

4. Spectroscopic Results

4.1. IR Spectra. The infrared spectrum of F^-CH_4 is shown in Figure 5. As reported previously,^{11,13} the parallel band, with a prominent head at 2525 cm^{-1} , is due to the stretching vibration of the H-bonded CH group ($\nu_{hb}(a_1)$), whereas the higher-frequency perpendicular band is due to an asymmetric stretching vibration of the three nonbonded CH groups ($\nu_3(e)$). The $\nu_3(a_1)$ band, corresponding to the symmetric stretching vibration of the nonbonded CH groups, is predicted to be IR weak (intensity 0.003 times that of the H-bonded CH stretching) and is not apparent in the spectrum.

The stretching potential curve for the H-bonded CH group is very anharmonic (as a result of incipient proton transfer from CH_4 to F^-), and for this reason the scaled harmonic frequency for $\nu_{hb}(a_1)$ significantly overestimates the actual value. Elsewhere we have developed an ab initio 1D potential energy curve for the H-bonded CH stretching that gave a better estimate of the $\nu_{hb}(a_1)$ frequency.¹³ As part of the current work, anharmonic vibrational frequencies for F^-CH_4 were calculated using the

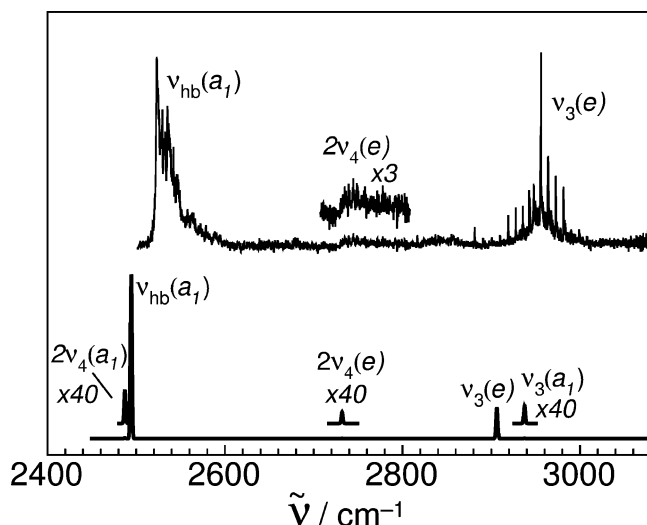


Figure 5. Experimental IR spectrum of F^-CH_4 . A stick spectrum generated using anharmonic VSCF-PT2 frequencies and intensities for fundamentals and overtones is also shown.

vibrational self-consistent field method with second-order perturbation correction (the VSCF-PT2 method).³⁶ Because the VSCF method couples normal modes (in this case restricted to pairs of modes) it should satisfactorily describe Fermi resonances between pairs of interacting levels.

The experimental, scaled harmonic, and VSCF-PT2 frequencies for CH_4 and F^-CH_4 are summarized in Table 1. The VSCF-PT2 ν_{hb} frequency (2494 cm^{-1}) is in much better agreement with the experimental value (2535 cm^{-1}) than is the scaled harmonic frequency (2645 cm^{-1}). The success of the VSCF-PT2 calculations in reproducing the experimental results can be judged from Figure 5, where the experimental spectrum and a simulated spectrum based on the VSCF-PT2 frequencies and intensities are compared.

We note that in the F^-CH_4 spectrum there is a weak feature at 2745 cm^{-1} (magnified in Figure 5) that can be assigned to the a_1 component of $2\nu_4(e)$ gaining IR intensity through Fermi interaction with ν_{hb} . This assignment is supported by the VSCF-PT2 calculations, which predict that $2\nu_4(e)$ occurs at 2732 cm^{-1} . Predicted frequencies, and in some cases intensities, of other overtone and combination levels with appropriate a_1 symmetry for interacting with $\nu_{hb}(a_1)$ are also listed in Table 1. Generally, the other levels are well separated in energy from ν_{hb} and presumably are not sufficiently mixed to derive appreciable IR intensity. For example, there is no evidence for the a_1 component

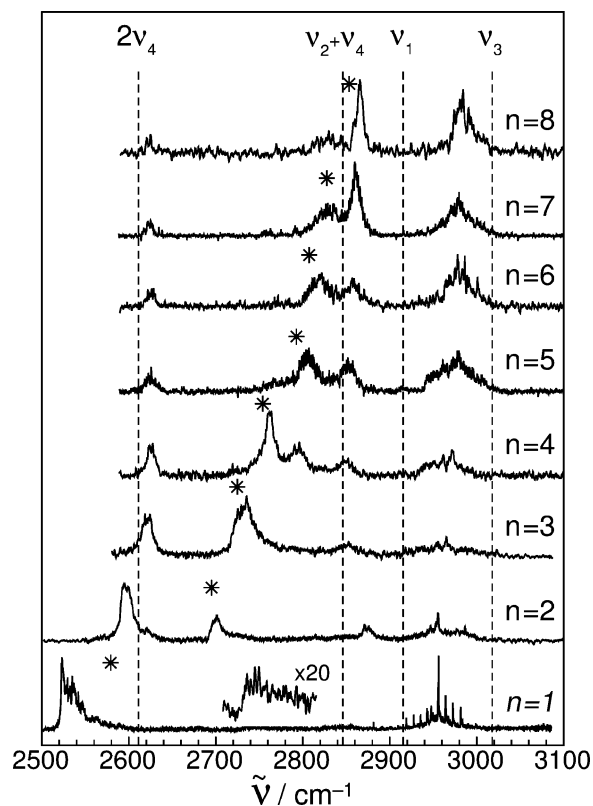


Figure 6. Infrared spectra of $F^-(CH_4)_n$, $n = 1-8$. Dashed lines at 2612 , 2845 , 2917 , and 3020 cm^{-1} mark the $2\nu_4$, $\nu_2 + \nu_4$, ν_1 , and ν_3 bands of CH_4 .⁴¹ Asterisks indicate the center of gravity of spectral density below 2910 cm^{-1} and correspond to deperturbed $\nu_{hb}(a_1)$ frequencies (Table 2).

of $\nu_2(e) + \nu_4(e)$ predicted to lie at 2886 cm^{-1} , well above $\nu_{hb}(a_1)$ (and possibly within the wing of the $\nu_3(e)$ band). The a_1 component of $2\nu_2(e)$ (3068 cm^{-1}) also lies well above $\nu_{hb}(a_1)$, whereas $2\nu_4(a_1)$ (2472 cm^{-1}) is predicted to lie below the investigated spectral range.

4.2. Larger Clusters. Infrared spectra of $F^-(CH_4)_n$ ($n = 1-8$) clusters in the CH stretching region are shown in Figure 6. Band wavenumbers are listed in Table 2. The $n = 2-8$ spectra each display four or five bands in the CH stretching region and are more complicated than the $n = 1$ spectrum. In each case, the highest-energy band clearly correlates with the $\nu_3(e)$ transition in the $n = 1$ spectrum. Despite losing the sharp Q-branch structure, the $\nu_3(e)$ band retains a broad profile, and

TABLE 1: Fundamental, Overtone, and Combination Levels for CH_4 and F^-CH_4 .^a

CH_4 level (T_d)	CH_4 expt	CH_4 VSCF-PT2	F^-CH_4 level (C_{3v})	symmetry in C_{3v}	F^-CH_4 expt	F^-CH_4 scaled	F^-CH_4 VSCF-PT2
$\nu_4(t_2)$	1306	1315	$\nu_4(a_1)$	a_1		1236	1269
			$\nu_4(e)$	e		1352	1362
$\nu_2(e)$	1524	1539	$\nu_2(e)$	e		1534	1557
$2\nu_4(t_2)$	2612	2621	$2\nu_4(a_1)$	a_1		2472 ^b	2487(3.5)
			$\nu_4(a_1) + \nu_4(e)$	e		2588 ^b	2631 ^b
			$2\nu_4(e)$	$a_1 + e$	2745	2704 ^b	2732(0.6)
$\nu_1(a_1)$	2917	2953	$\nu_{hb}(a_1)$	a_1	2535	2645	2494(671)
$\nu_2(e) + \nu_4(t_2)$	2845	2854 ^b	$\nu_2(e) + \nu_4(a_1)$	e		2770 ^b	2826 ^b
			$\nu_2(e) + \nu_4(e)$	$a_1 + a_2 + e$		2886 ^b	2919 ^b
$\nu_3(t_2)$	3019	3104	$\nu_3(e)$	e	2956	2967	2906(68)
			$\nu_3(a_1)$	a_1		2904	2937(1.9)
$2\nu_2(e)$	3072	3077	$2\nu_2(e)$	$a_1 + e$		3068 ^b	3108(2.8)

^a Scaled wavenumbers for stretch and bend fundamentals are obtained by multiplying harmonic ab initio values by 0.9398 and 0.9616 (the factors required to reconcile CH_4 ab initio and experimental frequencies from refs 41 and 42) Unscaled anharmonic VSCF-PT2 frequencies are also listed. ^b Frequencies of these combination levels are taken as the sum of the frequencies of the fundamentals.

TABLE 2: Band Wavenumbers for $F^-(CH_4)_n$, $n = 1-8$ ($\pm 5 \text{ cm}^{-1}$)^a

<i>n</i>	$\bar{\nu}_{hb}(a_1)$		$\nu_3(e)$		
1	2535 (1.0)	2745 (0.07)	2583	2956	
2	2596 (1.0)	2701 (0.45)	2872 (0.27)	2696 2955	
3	2622 (0.69)	2736 (1.0)	2853 (0.21)	2713 2965	
4	2625 (0.46)	2762 (1.0)	2796 (0.51)	2851 (0.27)	2760 2973
5	2625 (0.50)	2767 (0.33)	2807 (1.0)	2852 (0.86)	2797 2979
6	2625 (0.43)	2770 (0.14)	2821 (1.0)	2857 (0.82)	2808 2979
7	2625 (0.19)		2830 (0.45)	2860 (1.0)	2827 2980
8	2625 (0.26)		2830 (0.27)	2866 (1.0)	2858 2984

^a Relative intensities for bands in the 2500–2900 cm^{-1} range are given in brackets (estimated uncertainties $\pm 20\%$). The $\bar{\nu}_{hb}(a_1)$ values are deperturbed frequencies of the H-bonded CH stretching vibration obtained using the approach described in section 4.2.

as n increases, it gradually shifts to a higher frequency back toward the $\nu_3(t_2)$ band of bare CH_4 .

Below the $\nu_3(e)$ band, in the 2500–2900 cm^{-1} range, the $n = 1-8$ spectra exhibit a more complicated pattern and a pronounced size dependence. As n increases, the $\nu_{hb}(a_1)$ band shifts to a higher frequency and splits into several bands. This behavior is unexpected. For $F^-(CH_4)_n$ clusters containing equivalent CH_4 molecules H bonded to F^- , one might expect to see a single $\nu_{hb}(a_1)$ band that shifts back to a higher frequency as n increases, reflecting a weakening of the intermolecular H bonds. Indeed, this is the situation for the $\text{Cl}^-(CH_4)_n$, $n = 1-10$, clusters where the $\nu_{hb}(a_1)$ bands are red-shifted much less than for the $F^-(CH_4)_n$ clusters.¹⁴

The complexities in the $n = 2-8$ spectra can be explained most convincingly by Fermi resonances between the $\nu_{hb}(a_1)$ level and CH_4 bending overtone and combination levels. As shown in Figure 6, the $2\nu_4$ overtone and $\nu_2 + \nu_4$ combination levels of CH_4 lie in the same spectral region as the observed bands (2600–2850 cm^{-1}). We expect that as the clusters become larger the $F^-\cdots\text{CH}_4$ H bonds will weaken and the H-bonded CH stretching levels will shift to a higher frequency back toward the $\nu_1(a_1)$ band of the free CH_4 molecule. As this occurs, $\nu_{hb}(a_1)$ comes into resonance with the $2\nu_4$ overtone and $\nu_2 + \nu_4$ combination levels, resulting in mixed levels whose IR intensities depend on the admixture of $\nu_{hb}(a_1)$.

For $n = 2$, three distinct bands occur in the region below the $\nu_3(e)$ band, which, in order of increasing frequency, would predominately be of $\nu_{hb}(a_1)$, $2\nu_4(e)$, and $\nu_2(e) + \nu_4(e)$ character. The same three bands occur for $n = 3$, although it appears that the $\nu_{hb}(a_1)$ level now lies above the $2\nu_4(e)$ overtone because the middle band is now the most intense. As n increases, the strongest band, presumably associated with a transition to the level with the most $\nu_{hb}(a_1)$ character, steadily increases in frequency and for $n = 8$ eventually appears as a narrow, dominant peak with a width of 10 cm^{-1} . There is a corresponding frequency decrease for the two bands associated with transitions to levels of predominately $2\nu_4(e)$ and $\nu_2(e) + \nu_4(e)$ character, until at $n = 8$ they are close in frequency to the overtone and combination levels of the bare CH_4 molecule (Figure 6).

The $n = 4$ spectrum has an additional band at 2796 cm^{-1} of uncertain origin that may be associated with a combination level involving $2\nu_4(a_1)$ and one quantum of an intermolecular stretch that interacts effectively with $\nu_{hb}(a_1)$ when the energy separation is small. Remnants of this band appear in the $n = 5$ and 6 spectra at 2767 and 2770 cm^{-1} , respectively.

The zeroth-order $\nu_{hb}(a_1)$ frequencies for the $n = 1-8$ clusters can be estimated assuming that transitions in the 2500–2900 cm^{-1} range derive their IR intensity solely from the admixture

of $\nu_{hb}(a_1)$ in the makeup of the upper state. The zeroth-order frequency $\bar{\nu}_{hb}(a_1)$ is then given by

$$\bar{\nu}_{hb}(a_1) = \frac{\sum_{i=1}^n \nu_i I_i}{\sum_{i=1}^n I_i} \quad (1)$$

where ν_i and I_i are the frequency and intensity of the i^{th} band. In practice, the sums are replaced by integrals so that the unperturbed $\nu_{hb}(a_1)$ frequency corresponds to the center of gravity of the spectral density, that is,

$$\bar{\nu}_{hb}(a_1) = \frac{\int_{\nu_1}^{\nu_2} \nu I(\nu) d\nu}{\int_{\nu_1}^{\nu_2} I(\nu) d\nu} \quad (2)$$

where $I(\nu)$ is the intensity at frequency ν and the integration range is 2500 to 2910 cm^{-1} . The $\bar{\nu}_{hb}(a_1)$ values deduced from the $n = 1-8$ spectra are marked by asterisks in Figure 6 and listed in Table 2. The estimations are obviously sensitive to the band intensities and will be affected by saturation of the weaker transitions. Estimated errors are $\pm 30 \text{ cm}^{-1}$.

The $\bar{\nu}_{hb}(a_1)$ frequencies increase steadily with n , reflecting a progressive weakening of the $F^-\cdots\text{CH}_4$ H bonds as more CH_4 molecules are coordinated with the F^- . The situation is similar for the $\text{Cl}^-(CH_4)_n$, $n = 1-10$, clusters,¹⁴ although in that case the $\nu_{hb}(a_1)$ red shifts are much smaller so that Fermi resonances play a negligible role. The migration of the $\nu_{hb}(a_1)$ band to a higher frequency as n increases appears to be a general feature of H-bonded anion clusters (e.g., refs 14, 27, 28, and 43).

One of the remarkable features of the $F^-(CH_4)_n$ series is the simplicity of the $n = 1$ and 8 spectra compared to the $n = 2-7$ spectra. The explanation is that for $n = 1$ the ν_{hb} level is too low in frequency to interact effectively with the CH_4 bending overtone and combination levels, whereas for $n = 8$ it lies too high.

Although the multiple bands of the $F^-(CH_4)_n$ clusters in the 2500–2900 cm^{-1} range can be explained by Fermi resonances, it is worth considering other explanations. These include the following:

(a) The bands are associated with different combinations of $\nu_{hb}(a_1)$ vibrations localized on the CH_4 ligands that have different frequencies due to coupling through the F^- anion.

(b) Each of the bands is associated with CH_4 molecules in different H-bonding environments. That is, in each sized cluster, some of the $F^-\cdots\text{CH}_4$ H bonds are stronger than others.

(c) For each cluster size, there are several isomeric forms having different $\nu_{hb}(a_1)$ frequencies.

Considering option a first, we recall that a $F^-(CH_4)_n$ cluster containing n equivalent methane molecules possesses n distinct $\nu_{hb}(a_1)$ vibrational modes, each with a slightly different frequency. For example, the $n = 2$ cluster shown in Figure 2 has symmetric and antisymmetric $\nu_{hb}(a_1)$ stretches. Comparisons between the experimental and predicted spectra are made in Figure 7. Although the calculations predict two peaks arising from H-bonded CH stretches for the $n = 2$ and 3 clusters, the spacings ($\sim 30 \text{ cm}^{-1}$ in both cases) are substantially less than the observed spacings (100 and 115 cm^{-1}). There are also significant differences between the calculated and experimental intensities. For $n = 2$, the two bands are predicted to have comparable intensities, yet in the experimental spectrum the

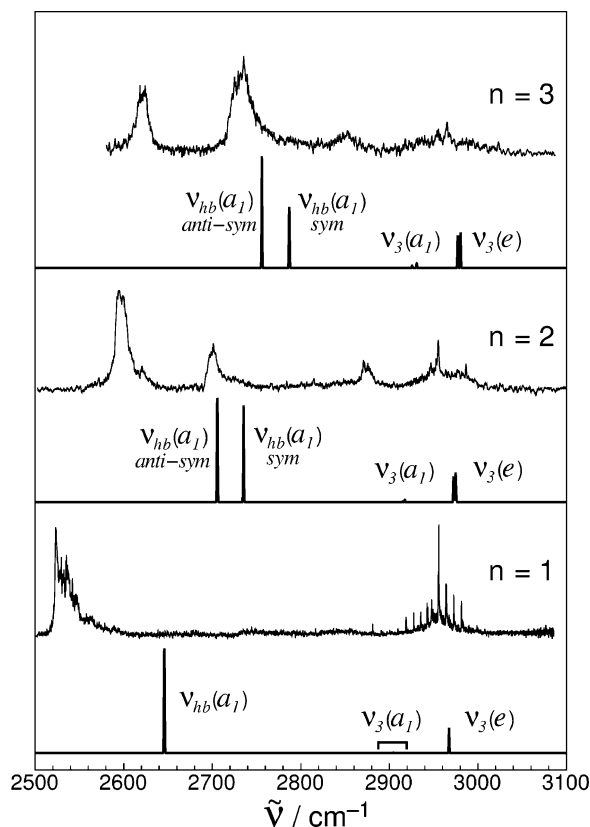


Figure 7. Infrared spectra of $F^--(CH_4)_n$, $n = 1-3$, in the CH stretching region. Stick spectra generated using scaled harmonic ab initio frequencies are also shown. Ab initio frequencies were scaled by the factor (0.9398) required to reconcile calculated and experimental stretching frequencies for free CH_4 .

lower-energy band is two to three times more intense than the higher-energy band. Moreover, for $n = 3$, the lower band is slightly weaker than the upper band, whereas the calculations predict that it should have twice the upper band's intensity. It is worth noting that vibrational excitation of the low-frequency intermolecular modes can affect the intensities of the $\nu_{hb}(a_1)$ modes. For example, excitation of the lowest-frequency bending mode of $F^-(CH_4)_2$ will incline the complex toward linearity, reducing the intensity of the symmetric combination (higher-frequency band). This effect is revealed for $F^-(CH_4)_2$ in Figure 3 where the ratio for the IR intensities of the symmetric and antisymmetric $\nu_{hb}(a_1)$ modes is plotted as a function of the bending angle. Because the lowest-frequency bending mode will likely be excited in a considerable fraction of the experimentally probed clusters, it is probable that the symmetric $\nu_{hb}(a_1)$ band will appear only as a tail on the high-frequency side of the stronger antisymmetric $\nu_{hb}(a_1)$ band. In any case, option **a** is unlikely.

Options **b** and **c** also seem improbable given that ab initio calculations for $n = 2$ and 3 indicate that the CH_4 molecules bind to F^- by single, equivalent H bonds. Attempts to locate structures in which the methanes are not H bonded to the F^- were unsuccessful. This is unsurprising given that the $F^- \cdots CH_4$ bond ($D_0 \approx 2400 \text{ cm}^{-1}$)² is around 20 times stronger than the $CH_4 \cdots CH_4$ bond ($D_0 \approx 130 \text{ cm}^{-1}$).³⁷⁻⁴⁰ In the finite temperature clusters probed spectroscopically, the CH_4 molecules will certainly undergo torsional motions and move about with respect to one another. However, calculations for $F^-(CH_4)_2$ show that the CH stretching frequencies are insensitive to the torsional configuration and relative positions of the CH_4 molecules as

long they both remain H bonded to the F^- . A similar situation should prevail in the larger clusters.

5. Discussion

Previous studies have shown that the solvation structures of small hydrogen-bonded clusters can be deduced from IR spectra in conjunction with ab initio calculations. For example, the halide anion in $Cl^-(H_2O)_n$, $Br^-(H_2O)_n$, and $I^-(H_2O)_n$ resides on the surface of a hydrogen-bonded water network.¹⁹ This arrangement allows each H_2O molecule to act as a proton donor to the halide and to another H_2O molecule while at the same time acting as an H-bond acceptor. The comparable strengths of the water-water and water-halide hydrogen bonds favor the networked surface-solvation structures. In contrast, for halide-acetylene clusters ($Cl^-(C_2H_2)_n$, $Br^-(C_2H_2)_n$, and $I^-(C_2H_2)_n$), the C_2H_2 molecules H bond end-on to the halide anion and in this arrangement are unable to bond effectively with one another.²⁶⁻²⁸ Indeed, repulsive quadrupole-quadrupole forces serve to keep the C_2H_2 molecules apart. This leads to interior solvation structures where the halide is surrounded by linearly H-bonded C_2H_2 solvent molecules.

In the case of the F^-CH_4 clusters, because of the relative strengths of the fluoride-methane and methane-methane bonds ($D_0 \approx 2400$ and 130 cm^{-1} , respectively), one can expect that while space permits, the CH_4 molecules will attach directly to F^- . Furthermore, the methanes should pack next to one another because of weak methane-methane dispersion interactions and because in this arrangement they can concertedly polarize the halide. These features are apparent in the $n = 2$ and 3 ab initio structures (Figure 2).

In many respects, the halide-methane clusters are probably similar to the halide-rare gas atom clusters studied using photoelectron spectroscopy by Neumark and co-workers.⁴⁴⁻⁴⁶ For these RG_n-X^- species, which include Ar_n-Cl^- , Ar_n-Br^- , Ar_n-I^- , and Xe_n-I^- , the RG atoms adopt positions that maximize the number of halide \cdots RG and RG \cdots RG bonds. In the smaller clusters ($n < 6$), the RG atoms aggregate on one side of the halide ion, gradually encasing it as the number of RG atoms increases and eventually forming icosahedral-type structures containing 12-15 RG atoms in the first solvent shell.

Figure 8 illustrates putative close-packed structures for $F^-(CH_4)_n$, $n = 1-12$, clusters in which CH_4 molecules are attached to F^- by equivalent H bonds, forming structures that are analogous to the structures of the halide-rare gas atoms clusters. The calculated $n = 1-3$ structures shown in Figure 2 can be viewed as the first steps along a path that eventually leads to an icosahedron for $n = 12$. The 2nd to 6th CH_4 molecules are positioned in a primary five-membered ring, whereas the 7th to 11th ligands sit in a secondary ring. The 12th molecule caps the icosahedron. The $Cl^-(CH_4)_n$, $n = 1-10$, clusters were postulated to have close-packed structures similar to those shown in Figure 8.

The experimentally probed $F^-(CH_4)_n$ clusters are likely to be highly fluxional because, as discussed in section 3.1, torsional barriers of the methanes are very low, and the methane-methane bonds are easily broken. However, fluxionality may be reduced as more methanes are added, limiting the space available for each methane molecule.

The structures of the $F^-(CH_4)_n$ clusters illustrated in Figure 8 differ from those postulated by Hiraoka et al.,² who, on the basis of a small but sharp drop in the measured association enthalpies between $n = 6$ and 7 , decided that the $n = 6$ cluster has an octahedral structure. An alternative explanation for the abrupt drop in the association enthalpy at $n = 7$ (Figure 1) is

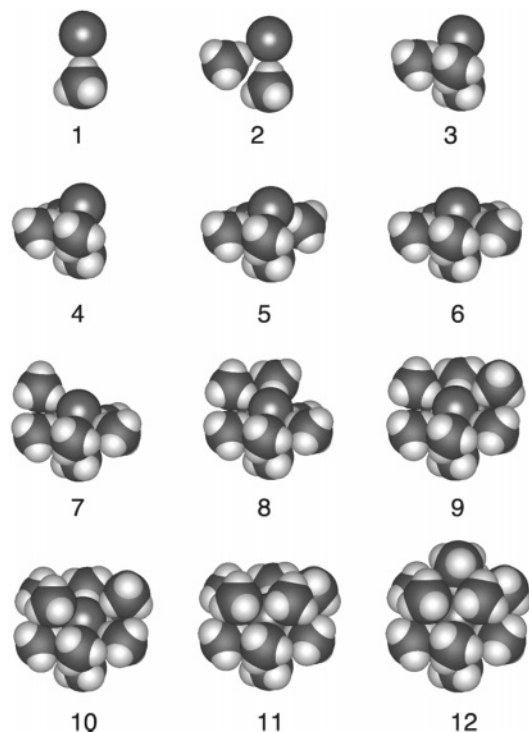


Figure 8. Postulated structures for $F^-(CH_4)_n$, $n = 1-12$, clusters.

that, as shown in Figure 8, the sixth ligand completes the first solvation ring, occupying an energetically favorable position, whereas the seventh ligand is added to the second ring, where it has fewer close neighbors to stabilize it. At this stage we are unable to explain a less distinct drop in the measured association enthalpies between $n = 8$ and 9, which was taken by Hiraoka et al. to indicate that the seventh and eighth CH_4 molecules fit into opposite pockets of an octahedral core.

It is interesting that the deperturbed ν_{hb} frequency of $F^-(CH_4)_8$ (2858 cm^{-1}) is similar to the ν_{hb} frequency of Cl^-CH_4 (2875 cm^{-1}), which, assuming that the red shift of the H-bonded CH stretching is related to the H-bond strength, suggests that the H-bond strengths are similar in both cases. Indeed, the measured association enthalpies for $F^-(CH_4)_8$ (2.9 kcal/mol) and Cl^-CH_4 (3.8 kcal/mol) are relatively close to one another.

The manner in which the ν_{hb} level tunes into resonance with the CH_4 bend overtone and combination levels as the ionic H bonds weaken is reminiscent of the situation for the halide-water dimers (Cl^-H_2O , Br^-H_2O , and I^-H_2O).²¹ For Br^-H_2O , the H-bonded OH stretching band is almost resonant with the H_2O bending overtone, and two bands of comparable intensity occur in the IR spectrum. For Cl^-H_2O and I^-H_2O , the H-bonded OH stretch lies respectively well below and well above the bending overtone so that the Fermi coupling is weak, and in each case, the spectrum is dominated by the strong ν_{hb} transition with the bending overtone appearing as a much smaller peak.

The $Cl^-H_2O-(CCl_4)_n$ systems supply yet another example of Fermi tuning/detuning.³⁰ For the $n = 1$ complex, there is a pronounced resonance between the H-bonded OH stretching vibration of the water molecule and two quanta of the water bend vibration. As additional CCl_4 molecules are added, the H-bonded OH stretching vibration increases in frequency (as a result of charge delocalization onto the CCl_4 molecules), and the resonance becomes progressively weaker.

Finally, we remark on the vibrational red shifts for the $F^-(CH_4)_n$ clusters. As n increases, the IR bands associated

with the H-bonded X-H groups shift progressively to the blue, back toward the stretching frequency for the free methane molecule. A similar situation occurs for the $Cl^-(CH_4)_n$ clusters.¹⁴ This progressive blue shift (or diminishing red shift) accompanies a progressive weakening of the halide-methane hydrogen bonds, a trend that is discernible in the measured bond enthalpies for the $F^-(CH_4)_n$ clusters (Figure 1).² The red shift in the frequency of the H-bonded X-H group for a CH_4 molecule attached to F^- can be explained in terms of a combination of electrostatic and charge-transfer effects.⁴⁷⁻⁴⁹ The incremental addition of CH_4 ligands about a halide anion core is expected to reduce both contributions. In regard to the electrostatic contribution, the electric field experienced by any one methane ligand in the $F^-(CH_4)_{n+1}$ cluster will be lower than that experienced by each methane molecule in the $F^-(CH_4)_n$ cluster. This is principally because polarization of the methane molecules will tend to reduce the electric field arising from the charge on the fluoride anion. Thus, the vibrational band shift due to electrostatic causes will be reduced in the $F^-(CH_4)_{n+1}$ cluster compared to that in the $F^-(CH_4)_n$ cluster. Regarding the charge-transfer effects, the incremental addition of solvent methane molecules to the fluoride anion will progressively reduce the charge residing on the fluoride anion (as charge is transferred into the σ^* antibonding orbital of the H-bonded X-H groups). Therefore, as n increases there will be a reduction in the charge available for transfer to any one methane. Again, the outcome is a reduction in the red shift of the H-bonded X-H groups (that is, an incremental blue shift) as the cluster becomes larger.

Acknowledgment. We are grateful to the Australian Research Council and the University of Melbourne for financial support. M.S.G. acknowledges an international travel grant from the U.S. National Science Foundation and a Senior Fulbright Fellowship that made this collaboration possible. Calculations were supported by a grant from the Air Force Office of Scientific Research and by a grant of computer time from the High Performance Computing Modernization Program (HPCMP) of the Department of Defense. J.M.L. thanks the Wilmore Foundation for support during sabbatical leave at the University of Melbourne and support by the U.S. National Science Foundation under grant no. CHE-0415859.

Supporting Information Available: Harmonic vibrational frequencies and intensities for $F^-(CH_4)_n$ ($n = 1-3$) calculated at the MP2/6-311++G(2df 2p) level. This material is available free of charge via the Internet at <http://pubs.acs.org>.

References and Notes

- (1) Evans, D. H.; Keese, R. G.; Castleman, A. W., Jr. *J. Chem. Phys.* **1987**, *86* (5), 2927-31.
- (2) Hiraoka, K.; Mizuno, T.; Iino, T.; Eguchi, D.; Yamabe, S. *J. Phys. Chem. A* **2001**, *105*, 4887-4893.
- (3) Yates, B. F.; Schaefer, H. F., III; Lee, T. J.; Rice, J. E. *J. Am. Chem. Soc.* **1988**, *110*, 6327-6332.
- (4) Novoa, J. J.; Whangbo, M. H.; Williams, J. M. *Chem. Phys. Lett.* **1991**, *180*, 241-248.
- (5) Xantheas, S. S.; Dunning, T. H., Jr. *J. Phys. Chem.* **1994**, *98*, 13 489-13 497.
- (6) Xantheas, S. S. *J. Phys. Chem.* **1996**, *100*, 9703-9713.
- (7) Del Bene, J. E.; Jordan, M. J. T. *Spectrochim. Acta, Part A* **1999**, *55*, 719-729.
- (8) Nemukhin, A. V.; Aleksandr, A. G.; Firsov, D. A. *Mendeleev Commun. Electronic Version*, 213-215.
- (9) Kawahara, S.-i.; Uchimaru, T.; Taira, K. *Chem. Phys.* **2001**, *273*, 207-216.
- (10) Chaban, G. M.; Xantheas, S. S.; Gerber, R. B. *J. Phys. Chem. A* **2003**, *107*, 4952-4956.

- (11) Wild, D. A.; Loh, Z. M.; Bieske, E. J. *Int. J. Mass Spectrom.* **2002**, *220*, 273–280.
- (12) Wild, D. A.; Loh, Z. M.; Wolyneec, P. P.; Weiser, P. S.; Bieske, E. *J. Chem. Phys. Lett.* **2000**, *332*, 531–537.
- (13) Loh, Z. M.; Wilson, R. L.; Wild, D. A.; Bieske, E. J.; Gordon, M. S. *Aust. J. Chem.* **2004**, *57*, 1157–1160.
- (14) Loh, Z. M.; Wilson, R. L.; Bieske, E. J.; Gordon, M. S. *J. Phys. Chem. A* **2005**, *109*, 8481–8486.
- (15) Weiser, P. S.; Wild, D. A.; Wolyneec, P. P.; Bieske, E. J. *J. Phys. Chem. A* **2000**, *104*, 2562–2566.
- (16) Ayotte, P.; Bailey, C. G.; Johnson, M. A. *J. Phys. Chem. A* **1998**, *102*, 3067–3071.
- (17) Ayotte, P.; Kelley, J. A.; Nielsen, S. B.; Johnson, M. A. *Chem. Phys. Lett.* **2000**, *316*, 455–459.
- (18) Ayotte, P.; Nielsen, S. B.; Weddle, G. H.; Johnson, M. A.; Xantheas, S. S. *J. Phys. Chem. A* **1999**, *103*, 10665–10669.
- (19) Ayotte, P.; Weddle, G. H.; Johnson, M. A. *J. Chem. Phys.* **1999**, *110*, 7129–7132.
- (20) Ayotte, P.; Weddle, G. H.; Kim, J.; Johnson, M. A. *Chem. Phys.* **1998**, *239*, 485–491.
- (21) Ayotte, P.; Weddle, G. H.; Kim, J.; Johnson, M. A. *J. Am. Chem. Soc.* **1998**, *120*, 12 361–12 362.
- (22) Cabarcos, O. M.; Weinheimer, C. J.; Lisy, J. M.; Xantheas, S. S. *J. Chem. Phys.* **1999**, *110*, 5–8.
- (23) Caldwell, G.; Kebarle, P. *Can. J. Chem.* **1985**, *63*, 1399–1406.
- (24) Kawaguchi, K.; Hirota, E. *J. Chem. Phys.* **1986**, *84*, 2953–2960.
- (25) Kawaguchi, K.; Hirota, E. *J. Chem. Phys.* **1987**, *87*, 6838–6841.
- (26) Weiser, P. S.; Wild, D. A.; Bieske, E. J. *Chem. Phys. Lett.* **1999**, *299*, 303–308.
- (27) Weiser, P. S.; Wild, D. A.; Bieske, E. J. *J. Chem. Phys.* **1999**, *110*, 9443–9449.
- (28) Wild, D. A.; Milley, P. J.; Loh, Z. M.; Weiser, P. S.; Bieske, E. J. *Chem. Phys. Lett.* **2000**, *323*, 49–54.
- (29) Cabarcos, O. M.; Weinheimer, C. J.; Martinez, T. J.; Lisy, J. M. *J. Chem. Phys.* **1999**, *110*, 9516–9526.
- (30) Robertson, W.; Weddle, G.; Kelley, J.; Johnson, M. *J. Phys. Chem. A* **2002**, *106*, 1205–1209.
- (31) Nielsen, S. B.; Ayotte, P.; Kelley, J. A.; Johnson, M. A. *J. Chem. Phys.* **1999**, *111*, 9593–9599.
- (32) Robertson, W. H.; Kelley, J. A.; Johnson, M. A. *J. Chem. Phys.* **2000**, *113*, 7879–7884.
- (33) Wilson, R.; Loh, Z.; Wild, D.; Thompson, C.; Schuder, M.D.; Lisy, J.; Bieske, E. *Phys. Chem. Chem. Phys.* **2005**, *7*, 3419–3425.
- (34) Weber, J.; Schneider, H. *J. Chem. Phys.* **2004**, *120*, 10056–10061.
- (35) Schmidt, M. W.; Baldrige, K. K.; Boatz, J. A.; Elbert, S. T.; Gordon, M. S.; Jensen, J. H.; Koseki, S.; Matsunaga, N.; Nguyen, K. A.; Shujun, S.; Windus, T. L.; Dupuis, M.; Montgomery, J. A., Jr. *J. Comput. Chem.* **1993**, *14*, 1347–63.
- (36) Chaban, G. M.; Jung, J. O.; Gerber, R. B. *J. Chem. Phys.* **1999**, *111*, 1823–1829.
- (37) Sherwood, A. E.; Prausnitz, J. M. *J. Chem. Phys.* **1964**, *41*, 429–37.
- (38) Matthews, G. P.; Smith, E. B. *Mol. Phys.* **1976**, *32*, 1719–1729.
- (39) Szczesniak, M. M.; Chalasinski, G.; Cybulski, S. M.; Scheiner, S. *J. Chem. Phys.* **1990**, *93*, 4243–53.
- (40) Tsuzuki, S.; Uchimaru, T.; Tanabe, K. *Chem. Phys. Lett.* **1998**, *287*, 327–332.
- (41) Toth, R. A.; Brown, L. R.; Hunt, R. H.; Rothman, L. S. *Appl. Opt.* **1981**, *20*, 932–5.
- (42) Herzberg, G. *Infrared and Raman Spectra of Polyatomic Molecules. Molecular Spectra and Molecular Structure*; Krieger Publishing: Malabar, FL, 1991; Vol. 2.
- (43) Wild, D. A.; Weiser, P. S.; Loh, Z. M.; Bieske, E. J. *J. Phys. Chem. A* **2002**, *106*, 906–910.
- (44) Lenzer, T.; Yourshaw, I.; Furlanetto, M. R.; Pivonka, N. L.; Neumark, D. M. *J. Chem. Phys.* **2001**, *115*, 3578–3589.
- (45) Pivonka, N. L.; Lenzer, T.; Furlanetto, M. R.; Neumark, D. M. *Chem. Phys. Lett.* **2001**, *334*, 24–30.
- (46) Yourshaw, I.; Zhao, Y.; Neumark, D. M. *J. Chem. Phys.* **1996**, *105*, 351–373.
- (47) Morokuma, K. *Acc. Chem. Res.* **1977**, *10*, 294–300.
- (48) Reed, A.; Curtiss, L. A.; Weinhold, F. *Chem. Rev.* **1985**, *88*, 899–926.
- (49) Thompson, W.; Hynes, J. *J. Am. Chem. Soc.* **2000**, *122*, 6278–6286.